High-order couplings in geometric complex networks of neurons

A. Tlaie,[1,2,3] I. Leyva,[1,2] and I. Sendiña-Nadal[1,2]
[1]*Complex Systems Group & GISC, Universidad Rey Juan Carlos, 28933 Móstoles, Madrid, Spain*
[2]*Center for Biomedical Technology, Universidad Politécnica de Madrid, Madrid, Spain*
[3]*Department of Applied Mathematics and Statistics, ETSIT Aeronáuticos, Universidad Politécnica de Madrid, 28040 Madrid, Spain*

(Received 17 July 2019; revised manuscript received 26 September 2019; published 14 November 2019)

We explore the consequences of introducing higher-order interactions in a geometric complex network of Morris-Lecar neurons. We focus on the regime where traveling synchronization waves are observed from a first-neighbors-based coupling to evaluate the changes induced when higher-order dynamical interactions are included. We observe that the traveling-wave phenomenon gets enhanced by these interactions, allowing the activity to travel further in the system without generating pathological full synchronization states. This scheme could be a step toward a simple phenomenological modelization of neuroglial networks.

DOI: 10.1103/PhysRevE.100.052305

I. INTRODUCTION

The combination of complex networks and nonlinear dynamics has provided a solid framework for the study of a large number of very different real systems that can be analyzed as large ensembles of dynamical units with nontrivial connectivity patterns; these systems are as diverse as economics [1], genetics [2], social dynamics [3], and neuroscience [4].

Among all the possible collective features that can emerge in this context, synchronization is the most extensively studied, since it has been revealed as the fundamental mechanism in the transmission of information in all kinds of dynamical ensembles [5]. One of the fields where this perspective has led to new research lines is in neuroscientific applications. The neural system can be considered as a dynamical complex network in all its relevant scales, ranging from the microscopic, where the networked elements are single neurons [6,7], through the cortical column mesoscale [8], to the entire brain [4,9], with the brain areas acting as nodes of a functional network defined in terms of correlation levels.

However, even if synchronization is a key mechanism involved in the coordination of the neural ensemble, it is well known that exceedingly high levels of synchronization can destroy the overall complexity of the system, reducing its ability to process information and, eventually, leading to pathological states as epilepsy [10]. Therefore, a healthy synchronous functioning in the brain needs the existence of mechanisms of regulation, both structural and dynamical, to ensure the proper equilibrium between coordination and function segregation.

A plausible regulating mechanism is the astrocytes ensemble [11], whose role in brain performance is a long-standing problem in neuroscience. It is now known that astrocytes are involved in early synapse formation [12]. At the microscale, it is known that a single astrocyte can contact up to 10^5 synapses, meaning that these cells might be responsible for the modulation [13,14] of the electrical response of neurons sharing no anatomical connection at all [15–18] and, therefore, they could be the source of high-order interactions supporting coordination levels that overcome the outreach of direct neural connectivity. Several attempts have been made to model the neuroglial interaction [19,20], most of them focusing on the neuron-astrocyte pair or, more commonly, a triad of two neurons and an astrocyte [21,22]. Recent studies have gone further to consider the networked context, using detailed conductivity models [23–25]. They coincide in showing how the interaction of the astrocites ensemble with the neuron network can induce robust spatial synchronization in the neuronal ensemble surrounding the astrocytes [24–26] and in particular to enhance the propagation of activity waves [23]. These models are, however, mathematically and computationally costly [24], and therefore it will be useful to introduce a phenomenological model which is able to reproduce the observed effects of the glial ensemble over the neural network such that, while retaining the more relevant physiological aspects, it allows at the same time to move on to larger networks.

In this work we model the neural-glial ensemble as a geometrical network (similarly to those studied in Refs. [27–29]) with synaptic coupling, where the effect of the synaptic modulation of astrocytes is introduced using a high-order interaction formalism developed by Estrada *et al.* in Refs. [30–33]. It provides a solid quantitative mean to simulate and analyze the dynamics of a system in which these higher-order interactions are present. These effects are susceptible of revealing themselves particularly important in space embedded systems, where the Euclidean distances shape not only the probability of connection but also their weights. The high-order connectivity operator allows us to extend the usual first-neighbor interaction scheme that disregards higher-order interactions under the implicit assumption that if two nodes are not topologically connected they do not dynamically interact; such an assumption is no longer valid in a network of neurons whose communication is mediated by astrocytes.

The application of the high-order connectivity formalism to a complex network of synaptically connected neurons can provide insights about how introducing not only first but also second-neighbors interactions might be useful to comprehend

further details of the neuronal dynamics in a simple and mathematically well-defined way. We show how it enhances the appearance of synchronization waves, a mean for transmitting a dynamical activation throughout the system in a coherent way, but avoiding the neuronal hyper-synchronization disorder that would result from increasing a direct neural connectivity.

II. MODEL

The network consists of an ensemble of N neurons that are randomly seeded in a two-dimensional (2D) Euclidean square area of size $L \times L$. The nodes are connected following a distance-dependent geometric rule (we refer the reader to Refs. [34–36] for further discussion of the experimental relevance of these topologies), such that neuron i has a probability of establishing a link with neuron j [37–39]:

$$p_{ij} = p_0\, e^{-(\frac{r_{ij}}{l_c})}, \tag{1}$$

where p_0 is a normalization constant, r_{ij} is the Euclidean distance between i and j, and l_c the correlation length parameter that controls the typical outreach of the connections when constructing the network; low values of this parameter yield highly clustered, short-ranged networks, while standard Erdös-Rényi networks are obtained in the limit of large l_c. The neural connectivity is encoded in the correspondent adjacency matrix $A = \{a_{ij}\}$ such that $a_{ij} = 1$ means a physical connection between neurons i and j and $a_{ij} = 0$ otherwise. In this case, we used a symmetrical adjacency matrix, $a_{ij} = a_{ji}$, with a_{ij} structurally supporting a chemical synapse. We chose a_{ij} to be symmetrical because, although experimentally it has been evidenced that chemical interactions are unidirectional, the fact that the number of synapses is so enormous implies that the probability that the dendritic trees of two neurons can contact each other is not negligible. In addition, as we intend to model in a phenomenological way the effect of the glia-neuron interaction, the symmetrical form of the adjacency matrix will take into account that activity information flows in both directions. Furthermore, as we will show later, the synaptic conductance is modeled to be asymmetrical, so when both structure and dynamics are considered, the interaction is effectively directed.

Single-node dynamics is implemented as a Morris-Lecar neuron [40]:

$$\begin{aligned} C\dot{V}_i =& -g_{\mathrm{Ca}} M_\infty (V_i - V_{\mathrm{Ca}}) - g_K W_i (V_i - V_K) \\ & - g_l (V_i - V_l) + I_i + I_i^{\mathrm{ext}} \\ \dot{W}_i =& \phi\, \tau_W (W_\infty - W_i), \end{aligned} \tag{2}$$

where V_i and W_i are, respectively, the membrane potential (or active variable) and the fraction of open K^+ channels of the ith neuron, also known as the recovery variable; ϕ is a reference frequency, namely the inverse of the timescale for the recovery process. The parameters g_X and V_X account for the electric conductance and equilibrium potentials of the $X = \{K, \mathrm{Ca}, \mathrm{leaky}\}$ channels. An external current $I_i^{\mathrm{ext}} = I_0 + Q\xi_i$ is added, with $I_0 = 50$ mA chosen such that neurons are subthreshold to their natural firing regime, which, in this case, will be induced by the additive white Gaussian noise $Q\xi_i$ of zero mean and intensity Q. The injected current I_i is the total amount of current coming from network inputs that neuron i gets; mathematically, in the local coupling approximation, first-order neighbors contribute to the synaptic coupling, and therefore $I_i = \sum_{j\in\mathcal{N}_i} I_{ij}$, where $\mathcal{N}_i$ is the neighborhood of node i, that is, nodes j such that $a_{ij} = 1$.

TABLE I. Parameters used for the Morris-Lecar simulations.

C	20.0 μF/cm^2
g_{Ca}	4.0 μS/cm^2
g_K	8.0 μS/cm^2
g_l	2.0 μS/cm^2
V_{Ca}	120.0 mV
V_K	−80.0 mV
V_l	−60.0 mV
V_1	−1.2 mV
V_2	18.0 mV
V_3	2.0 mV
V_4	17.4 mV
ϕ	1/15
Q	0.5 mA
V_0	−59.0 mV

The direct synaptic interaction between presynaptic j neuron and excitatory postsynaptic i neuron is captured by the injected current I_{ij} [41–43]:

$$I_{ij} = \frac{\sigma}{K}[e^{-2(t-t_j)}(V_0 - V_i)], \tag{3}$$

with $t_j < t$ being the time of the last spike of node j. The synaptic conductance σ, normalized by the largest node degree K (number of connections that a given node has) present in the network, plays the role of coupling strength. This normalization is introduced in order to compare the dynamics of Eq. (3) independently of the specific connectivity density of the network. To have more details about this prescription, we refer the reader to Ref. [44].

Additionally, the channel voltage-dependent saturation values $M_\infty, W_\infty, \tau_W$ respond to hyperbolic functions dependent on V_i:

$$M_\infty(V_i) = \frac{1}{2}\left[1 + \tanh\left(\frac{V_i - V_1}{V_2}\right)\right], \tag{4}$$

$$W_\infty(V_i) = \frac{1}{2}\left[1 + \tanh\left(\frac{V_i - V_3}{V_4}\right)\right], \tag{5}$$

$$\tau_W(V_i) = \cosh\left(\frac{V_i - V_3}{2V_4}\right). \tag{6}$$

The explicit value of every parameter can be found in Table I.

In spatial, highly clustered homogeneous networks with reduced link range l_c, the coupling configuration described in Eq. (3) favors traveling-wave synchronization, as long as σ is high enough [39], a well-established feature of the spatially extended neural ensembles [20]. On the contrary, in the mean-field approximation limit, $l_c \to L$, only globally incoherent or coherent states are accessible [45]. In our model, as a balance between these two extrema, we intend to explore the potential enhancement effect of higher-order connectivity at the local spatial scale in the wave regime, as for example the glial ensemble has in the neural circuits that are not directly connected among them [18]. Therefore, following the same mathematical framework developed in Refs. [30–32],

we allow that the injection current I_i accounts for the contribution not only from neurons $j \in \mathcal{N}_i$ whose topological distance (also referred to as network distance, that is, the shortest-path length) is $d_{ij} = 1$, but also from neighbors at higher topological distances $d_{ij} > 1$, that is,

$$I_i = \sum_{d=1}^{D} d^{-\alpha} \left(\sum_{j|d_{ij}=d} I_{ij} \right), \tag{7}$$

where D is the maximal topological distance considered. The successively distant contributions to the injection synaptic current I_i are modulated by a geometrically decaying term, $d^{-\alpha}$, where the constant α is a suppression parameter for the distance-dependent coupling strength. Notice that when the summation is limited to the first order $D = 1$, the usual first-neighbors interaction is recovered.

III. SYNCHRONIZATION MEASURES

In order to quantify the level of coordination among the network firing events we count how many neurons fire within the same time window. First, the total simulation time T is divided in N_b bins of a convenient size τ, longer than the time duration of each individual spike but much shorter than the average interspike interval. Then the total simulation time is discretized as $T = N_b\tau$ and the time series of the dynamics of neuron ith is replaced by the binary series B_i, where $B_i(n) = 1$ if the ith neuron spiked within the nth time bin, and 0 otherwise, with $n = 1, \ldots, N_b$. This simplification of the dynamics ensures a fast an precise calculation of the ensemble statistics. Finally, the coherence between the spiking sequence of neurons i and j can be characterized with the quantity $s_{ij} \in [0, 1]$

$$s_{ij} = \frac{\sum_{n=1}^{N_b} B_i(n)B_j(n)}{\sqrt{\sum_{n=1}^{N_b} B_i(n) \sum_{n=1}^{N_b} B_j(n)}}, \tag{8}$$

where the term in the denominator is a normalization factor, such that $s_{ij} = 1$ implies full coincidence between the spike trains of neurons i and j. The ensemble average of s_{ij} is the global synchronization measure S, given by:

$$S = \langle s_{ij} \rangle = \frac{1}{N(N-1)} \sum_{i \neq j}^{N} s_{ij}. \tag{9}$$

However, as we are interested not only in global but also spatial local effects in the ensemble coherence from the high-order couplings, we use the coherence matrix s_{ij} to compute also the Euclidean local synchronization S_ρ, where only the correlation values s_{ij} of those neurons pairs which are closer to each other than a given distance ρ are taken into account, that is [39]:

$$S_\rho = \langle s_{ij} \rangle, \ \forall \{i, j\} \,|\, r_{ij} < \rho. \tag{10}$$

In our computations, all measures are averaged over five different realizations of networks.

It is expected that in the limit $\rho \to L$, $S_\rho \sim S$. High values of S_ρ would indicate that there are areas of size ρ firing synchronously. In the following, we use the difference $S_\rho - S$ as an indicator of the existence of either a traveling wave front (when $S_\rho - S$ is large) or global or null synchronization ($S_\rho \sim S$) otherwise. It should be noted that, in general, the difference $S_\rho - S$ is not *designed* as to solely detect wavelike activity. There can be cases (such as in strongly modular networks) in which a high discrepancy between S_ρ and S are due to a clustered but globally incoherent neuronal firing (that is, each module fires in a coherent fashion but the modular activity does not propagate to the rest of the network). In our particular case, neurons are in spatially embedded networks with homogeneous connectivity which is distance regulated and thus strong modularity can be discarded.

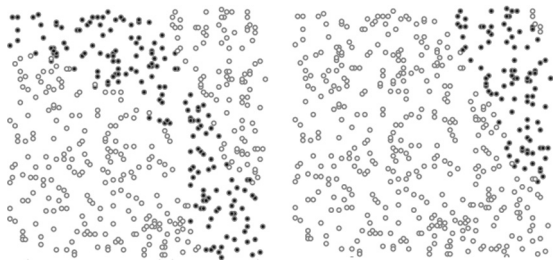

FIG. 1. Successive snapshots of the neurons' spiking activity in the traveling-wave synchronization mode. Filled dots represent spiking neurons while empty dots represent silent neurons. In the example the wave is propagating from the left to the right in a network of $N = 150$ Morris-Lecar neurons. Other parameters: $p_0 = 1.0$, $L = 50$, $l_c = 0.15$, $\sigma = 150$, $D = 1$.

IV. RESULTS

When just first-order interactions are present, this geometrical arrangement of neurons favors the propagation of traveling waves of neurons' spiking activity, supported by a highly clustered structure with a typically low link outreach [39]. To illustrate such propagation, in Fig. 1 we show two successive snapshots of an example where $l_c = 0.15$ and $\sigma = 150$. Here black dots represent spiking neurons while void dots portray those which are silent. The links between nodes are not included for clarity. This feature is quantified in Fig. 2, showing that this wavelike phenomenon is characterized by a local synchronization S_ρ (circles) larger than the global synchronization S (crosses), as it can be observed. The low value of the link outreach l_c prevents the system to reach full synchronization even when the coupling strength σ increases, whereas the local synchronization S_ρ grows much faster, indicating a reinforcement of the wave activity.

We now evaluate the effect of introducing higher-order contributions in the synaptic coupling in Eq. (7) received from neighbors at topological distance up to $D = 2$.

Results are collected in Fig. 3, where $S_\rho - S$ is plotted as a function of the conductance σ for different values of the suppression constant α, ranging between 0 and 3. For the sake of comparison, the curve for $D = 1$ is included (red circles). When $D > 1$, the higher the value of the suppression α, the weaker the influence from $D = 2$ neighbors. Therefore, we observe that for the higher suppression $\alpha = 3$ (purple squares), the behavior approaches the $D = 1$, and both curves overlap in almost the whole range of explored couplings up to $\sigma \sim 200$.

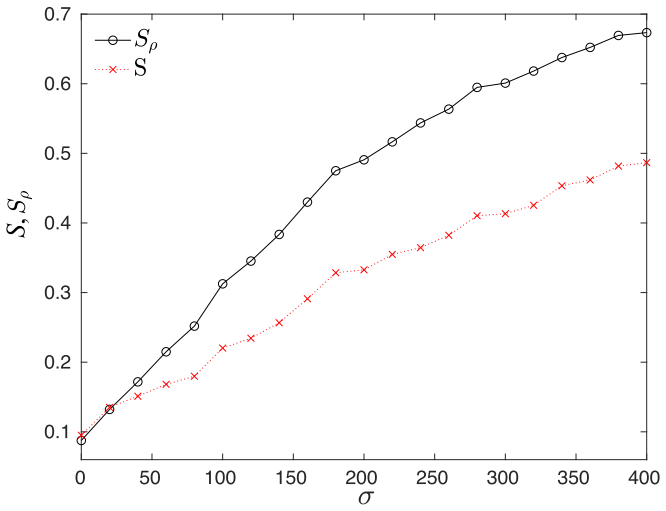

FIG. 2. Synchronization route as a function of the coupling strength σ for $l_c = 0.15$ and $D = 1$. Local synchronization S_ρ (black circles) computed with $\rho = 10$ and global synchronization (red crosses). Both series of data are averages over five $N = 150$ network realizations, with the connectivity scheme outlined in Sec. II.

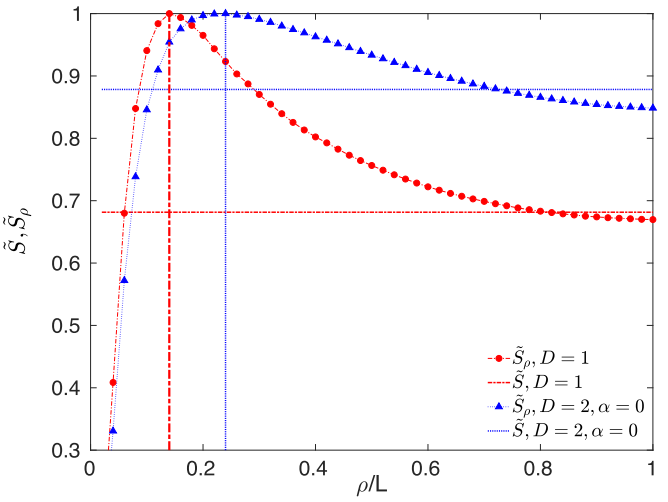

FIG. 4. Normalized local synchronization ($\tilde{S}_\rho$) values as a function of ρ/L for the two sets of parameter conditions defined by the gray circle in Fig. 3. Horizontal dashed lines mark the normalized values of the corresponding global synchronization. Vertical dashed lines mark the point defining the width of the traveling front. Each point is averaged over 10 network realizations.

However, as high-order effects become stronger for smaller values of α in Fig. 3, the S_ρ-S curves exhibit a maximum, located at lower values of the conductance σ. For instance, the curve for $D = 2$, $\alpha = 0$ (black triangles) peaks at $\sigma \sim 50$, while for the case $D = 1$ the $S_\rho - S$ difference is very small. The conclusion is that the introduction of another layer of interacting neighbors allows the propagation of traveling waves for coupling strengths where first-order interactions only supports incoherent activity. It can be deduced that this critical value of σ is related to the best communication efficiency of the spiking activity, given the constraints of a fixed topology and dynamical parameters. Notice that the traveling-wave feature implies a temporal ordering of the network's activity, as opposed to global synchronization (no temporal order) or incoherent activity (random spikes) and, therefore, this dynamical regime ensures a robust encoding of activity.

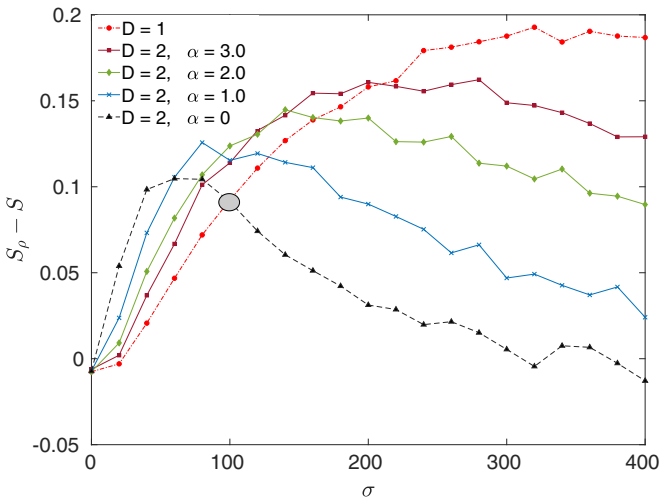

FIG. 3. Difference between local S_ρ and global S synchronization as a function of the coupling strength σ for different values of the suppression constant α and maximal topological distances $D = 1$ and $D = 2$. The gray circle highlights the intersection between the curves $D = 1$ and $(D = 2, \alpha = 0)$. Each point is an average over five network realizations. Same parameters as in Fig. 2.

To further explore the network activity and traveling-wave features, we focused on the coupling strength at which the two previously mentioned curves intersect (gray circle in Fig. 3, $\sigma \sim 100$), corresponding in both cases to wave propagation. However, we can observe that the wave-front features are also modified by the high-order effects. We analyzed these differences by varying the scale ρ at which the local synchronization S_ρ is measured for both cases at the crossing point. Figure 4 compares S_ρ for $D = 1$ (red circles) and $D = 2$, $\alpha = 0$ (blue triangles), normalized to their respective maxima, $\tilde{S}_\rho = S_\rho / \max(S_\rho)$, as a function of ρ/L, such that when ρ is of the same size L as the surface in which the network is seeded, the local synchronization statistically converges to the normalized global synchronization level [$\tilde{S} = S/\max(S)$] observed for each case (horizontal dashed lines). As expected, there is an optimal length scale ρ at which the local synchronization measure is maximum: Smaller scales undervalue the cluster of neurons spiking synchronously, while larger scales average neurons which are in different dynamical states. Therefore, the value of ρ at which $\tilde{S}_\rho$ peaks is an estimation of the wave-front width. Thus, as Fig. 4 indicates, higher-order interactions, for the same conductance value, allow the propagation of wider spiking waves, almost doubling the size with respect to $D = 1$. This could lead us to conclude that taking into account the direct influence of neighbors at larger topological distance allows the activity to be transmitted faster throughout the network, as more neurons are active in each wave front (while preserving the locality feature) and thus the wave front needs less time to cross the entire network.

V. CONCLUSIONS

In this work we have evidenced that the introduction of higher-order dynamical interactions in a ensemble of neurons with geometrical connectivity patterns leads to a faster and much more robust propagation of the activity through this spatially embedded system. This is so, due to the fact that, if at a given wave front there are more active neurons involved in the firing transmission, then it is more probable that the wave front will traverse the whole network, even if some of the neurons fail to transmit the signal. Thus, the transmission is more resistant to failures and, therefore, more robust. The propagation occurs as a traveling wave, whose wave front gets enhanced thanks to recruiting more neurons in the transmission. In addition, we have shown that higher-order dynamical interactions allow this kind of time-ordered synchronization for much lower coupling values than the case where only first-order neighbors are involved.

We hypothesize that this could be an innovative way of modeling the effects of neuroglial interaction, among other physical systems in which higher-order interactions need to be taken into account. Specifically, we argue that this mechanism of higher-order interactions could be a potent and computationally cheaper phenomenological approach to the detailed physiological models that can be found nowadays in the literature [23,25]. The central foundation for having chosen this particular mathematical formalism comes from a biological insight: Astrocytes have been evidenced to modulate up to $\approx 10^5$ synapses [46], while the majority of the neurons they interact with do not share an anatomical connection. This would imply that, while there is a given number of topological links in the network, some indirect ones would be present in the form of dynamical modulation, this role being played by astrocytes. As this is only a first step toward modeling the interplay between astrocytes and neurons in a network, we focused on establishing a solid base on which we will continue the research.

ACKNOWLEDGMENTS

Financial support from the Ministerio de Economía y Competitividad of Spain under Project No. FIS2017-84151-P and from the Group of Research of Excelence URJC-Banco de Santander is acknowledged. A.T. acknowledges support from the Comunidad de Madrid through the European Youth Employment Initiative and the Rey Juan Carlos University. Authors acknowledge the computational resources and assistance provided by CRESCO, the supercomputing center of ENEA in Portici, Italy.

[1] W. Souma, Y. Fujiwara, and H. Aoyama, Physica A **324**, 396 (2003).
[2] S. K. Sieberts and E. E. Schadt, Mamm. Gen. **18**, 389 (2007).
[3] P. V. Fellman, in *Unifying Themes in Complex Systems*, edited by A. Minai, D. Braha, and Y. Bar-Yam (Springer, Berlin, Heidelberg, 2010).
[4] E. Bullmore and O. Sporns, Nat. Rev. Neurosci. **10**, 186 (2009).
[5] A. Arenas, A. Díaz-Guilera, J. Kurths, Y. Moreno, and C. Zhou, Phys. Rep. **469**, 93 (2008).
[6] J.-P. Eckmann, O. Feinerman, L. Gruendlinger, E. Moses, J. Soriano, and T. Tlusty, Phys. Rep. **449**, 54 (2007).
[7] A. Kumar, S. Rotter, and A. Aertsen, Nat. Rev. Neurosci. **11**, 615 (2010).
[8] H. Zeng, Curr. Opin. Neurobiol. **50**, 154 (2018).
[9] V. M. Eguiluz, D. R. Chialvo, G. A. Cecchi, M. Baliki, and A. V. Apkarian, Phys. Rev. Lett. **94**, 018102 (2005).
[10] P. Jiruska, M. De Curtis, J. G. Jefferys, C. A. Schevon, S. J. Schiff, and K. Schindler, J. Physiol. **591**, 787 (2013).
[11] T. Fellin, O. Pascual, S. Gobbo, T. Pozzan, P. G. Haydon, and G. Carmignoto, Neuron **43**, 729 (2004).
[12] M. M. Bolton and C. Eroglu, Curr. Opin. Neurobiol. **19**, 491 (2009).
[13] W. J. Nett, S. H. Oloff, and K. D. Mccarthy, J. Neurophysiol. **87**, 528 (2002).
[14] M. C. Angulo, A. S. Kozlov, S. Charpak, and E. Audinat, J. Neurosci. **24**, 6920 (2004).
[15] G. Perea, M. Navarrete, and A. Araque, Trends Neurosci. **32**, 421 (2009).
[16] N. J. Allen and B. A. Barres, Nature (London) **457**, 675 (2009).
[17] F. Oschmann, H. Berry, K. Obermayer, and K. Lenk, Brain Res. Bull. **136**, 76 (2018).
[18] M. De Pittà, N. Brunel, and A. Volterra, Neuroscience **323**, 43 (2016).
[19] M. De Pitta and H. E. Berry, *Computational Glioscience* (Springer, Berlin, 2019).
[20] M. Santello, N. Toni, and A. Volterra, Nat. Neurosci. **22**, 154 (2019).
[21] Z. Sajedinia and S. Hélie, Comput. Intell. Neurosci. **2018**, 3689487 (2018).
[22] J.-J. Li, M.-M. Du, R. Wang, J.-Z. Lei, and Y. Wu, Int. J. Bifurcat. Chaos **26**, 1650138 (2016).
[23] M. Amiri, F. Bahrami, and M. Janahmadi, J. Theor. Biol. **292**, 60 (2012).
[24] O. Kanakov, S. Gordleeva, A. Ermolaeva, S. Jalan, and A. Zaikin, Phys. Rev. E **99**, 012418 (2019).
[25] S. Y. Gordleeva, A. V. Ermolaeva, I. A. Kastalskiy, and V. B. Kazantsev, Front. Physiol. **10**, 294 (2019).
[26] A. B. Porto-Pazos, N. Veiguela, P. Mesejo, M. Navarrete, A. Alvarellos, O. Ibáñez, A. Pazos, and A. Araque, PloS one **6**, e19109 (2011).
[27] M. Perc, New J. Phys. **7**, 252 (2005).
[28] X. Sun, M. Perc, Q. Lu, and J. Kurths, Chaos **18**, 023102 (2008).
[29] W.-J. Yuan, J.-F. Zhou, and C. Zhou, PLoS One **8**, e84644 (2013).
[30] E. Estrada and G. Silver, J. Math. Anal. Appl. **449**, 1581 (2017).
[31] E. Estrada, E. Hameed, N. Hatano, and M. Langer, Lin. Algeb. Appl. **523**, 307 (2017).
[32] E. Estrada, L. V. Gambuzza, and M. Frasca, SIAM J. Appl. Dynam. Syst. **17**, 672 (2018).
[33] J. H. Arias, J. Gómez-Gardeñes, S. Meloni, and E. Estrada, J. Theor. Biol. **453**, 1 (2018).

[34] D. de Santos-Sierra, I. Sendiña-Nadal, I. Leyva, J. A. Almendral, S. Anava, A. Ayali, D. Papo, and S. Boccaletti, PloS one **9**, e85828 (2014).
[35] O. Shefi, I. Golding, R. Segev, E. Ben-Jacob, and A. Ayali, Phys. Rev. E **66**, 021905 (2002).
[36] O. Stetter, D. Battaglia, J. Soriano, and T. Geisel, PLoS Comput. Biol. **8**, e1002653 (2012).
[37] M. Kaiser and C. C. Hilgetag, Phys. Rev. E **69**, 036103 (2004).
[38] M. Barthélemy, Phys. Rep. **499**, 1 (2011).
[39] I. Leyva, A. Navas, I. Sendiña-Nadal, J. M. Buldu, J. A. Almendral, and S. Boccaletti, Phys. Rev. E **84**, 065101(R) (2011).
[40] C. Morris and H. Lecar, Biophys. J. **35**, 193 (1981).
[41] M. J. Leone, B. N. Schurter, B. Letson, V. Booth, M. Zochowski, and C. G. Fink, Phys. Rev. E **91**, 032813 (2015).
[42] S. Mofakham, C. G. Fink, V. Booth, and M. R. Zochowski, Phys. Rev. E **94**, 042427 (2016).
[43] Z. G. Esfahani, L. L. Gollo, and A. Valizadeh, Sci. Rep. **6**, 23471 (2016).
[44] J. Gómez-Gardeñes, Y. Moreno, and A. Arenas, Phys. Rev. E **75**, 066106 (2007).
[45] R. Rosenbaum and B. Doiron, Phys. Rev. X **4**, 021039 (2014).
[46] E. A. Bushong, M. E. Martone, Y. Z. Jones, and M. H. Ellisman, J. Neurosci. **22**, 183 (2002).